Molecular Psychiatry (2014), 1–12

www.nature.com/mp

ORIGINAL ARTICLE

Glutathione deficit impairs myelin maturation: relevance for white matter integrity in schizophrenia patients

A Monin[1,2], PS Baumann[1,2,3], A Griffa[4,5], L Xin[6], R Mekle[7], M Fournier[1,2], C Butticaz[1,2], M Klaey[1,2], JH Cabungcal[1,2], P Steullet[1,2], C Ferrari[1,2], M Cuenod[1,2], R Gruetter[5,6], JP Thiran[4,5], P Hagmann[4,5], P Conus[2,3] and KQ Do[1,2]

Schizophrenia pathophysiology implies both abnormal redox control and dysconnectivity of the prefrontal cortex, partly related to oligodendrocyte and myelin impairments. As oligodendrocytes are highly vulnerable to altered redox state, we investigated the interplay between glutathione and myelin. In control subjects, multimodal brain imaging revealed a positive association between medial prefrontal glutathione levels and both white matter integrity and resting-state functional connectivity along the cingulum bundle. In early psychosis patients, only white matter integrity was correlated with glutathione levels. On the other side, in the prefrontal cortex of peripubertal mice with genetically impaired glutathione synthesis, mature oligodendrocyte numbers, as well as myelin markers, were decreased. At the molecular levels, under glutathione-deficit conditions induced by short hairpin RNA targeting the key glutathione synthesis enzyme, oligodendrocyte progenitors showed a decreased proliferation mediated by an upregulation of Fyn kinase activity, reversed by either the antioxidant *N*-acetylcysteine or Fyn kinase inhibitors. In addition, oligodendrocyte maturation was impaired. Interestingly, the regulation of Fyn mRNA and protein expression was also impaired in fibroblasts of patients deficient in glutathione synthesis. Thus, glutathione and redox regulation have a critical role in myelination processes and white matter maturation in the prefrontal cortex of rodent and human, a mechanism potentially disrupted in schizophrenia.

Molecular Psychiatry advance online publication, 26 August 2014; doi:10.1038/mp.2014.88

INTRODUCTION

Abnormalities in functional and structural brain connectivity are cardinal features of schizophrenia.[1] While functional dysconnectivity underlies alterations in neurotransmission system and brain activity, structural brain dysconnectivity includes impairments in synapses and myelination processes.[1] Recent research has focused on white matter and factors affecting its integrity. Findings from transcriptomics,[1–3] neuropathology[4–6] and neuroimaging[1,7–9] provide compelling evidence for alterations of oligodendrocytes and myelin in various subregions of the prefrontal cortex including anterior cingulate cortex of schizophrenia patients. Nevertheless, the underlying pathophysiological mechanisms are still elusive and their clarification would require investigating the early phase of the disease as their developmental emergence would be masked by chronicity.

Redox signaling has a key regulating role in many cellular and physiological processes. A redox dysregulation can affect cell proliferation/differentiation, energy metabolism and neurotransmission via an alteration of redox-sensitive protein function.[10] Converging data indicate a role for redox dysregulation in the pathophysiology of schizophrenia.[11–14] In some studies, decreased glutathione (GSH) levels, the main cellular non-protein antioxidant and redox regulator,[10,15] have been reported in the cerebrospinal fluid and prefrontal cortex of patients by using magnetic resonance spectroscopy (MRS)[16,17] and in *post-mortem* tissues.[14,18] We thus proposed that a redox dysregulation represents one hub on which converge various causal genetic and environmental risk factors during neurodevelopment, leading to structural and functional connectivity impairments. The genetic vulnerability factors involve either redox regulation genes directly affecting GSH metabolism,[19–22] or genes that indirectly lead to oxidative stress, including DISC1, PROD, G72, NRG and DTNBP1.[23–27] Environmental factors known to favor major psychiatric disorders also generate reactive oxygen species (ROS), which, if the redox regulation is impaired, will perturb the developing nervous system. As a consequence, two key systems essential for cognitive and affective functioning will be particularly affected: local microcircuits and long-range connections. More specifically, polymorphisms in the genes coding for the catalytic (GCLC)[20] and modifier (GCLM)[22] subunits of the glutamate-cysteine ligase (GCL), the rate-limiting enzyme for GSH synthesis, are associated with schizophrenia in case–control studies. The GAG trinucleotide repeat polymorphisms of *GCLC*, which are more frequent in patients ('GAG high-risk' genotypes),[20] are associated with changes in plasma thiol levels.[28] Compared with the 'GAG low-risk' genotypes, GCL activity and GSH content in fibroblasts are lower in 'GAG high-risk' genotypes under oxidative stress conditions.[20] These data prompted the investigation of *GCLM*

[1]Center for Psychiatric Neuroscience, Centre Hospitalier Universitaire Vaudois and University of Lausanne (CHUV-UNIL), Prilly-Lausanne, Switzerland; [2]Department of Psychiatry, Centre Hospitalier Universitaire Vaudois and University of Lausanne (CHUV-UNIL), Prilly-Lausanne, Switzerland; [3]Service of General Psychiatry, Centre Hospitalier Universitaire Vaudois and University of Lausanne (CHUV-UNIL), Prilly-Lausanne, Switzerland; [4]Signal Processing Laboratory, Ecole Polytechnique Fédérale de Lausanne (EPFL), Lausanne, Switzerland; [5]Department of Radiology, Centre Hospitalier Universitaire Vaudois and University of Lausanne (CHUV-UNIL), Lausanne, Switzerland; [6]Laboratory for Functional and Metabolic Imaging, Ecole Polytechnique Fédérale de Lausanne (EPFL), Lausanne, Switzerland and [7]Physikalisch-Technische Bundesanstalt, Berlin, Germany. Correspondence: Professor KQ Do, Department of Psychiatry, Center for Psychiatric Neuroscience, Centre Hospitalier Universitaire Vaudois and University of Lausanne, Prilly-Lausanne 1008, Switzerland.
E-mail: kim.do@chuv.ch
Received 13 February 2014; revised 30 April 2014; accepted 23 June 2014

knockout mice (*GCLM*-KO) as a model of schizophrenia. In developing and adult animals, brain GSH levels are decreased by 70%,[29] and *GCLM*-KO mice show signs of oxidative stress in discrete brain regions,[29,30] including the anterior cingulate cortex.[30] These mice present behavioral alterations such as impaired sensory gating, abnormal response to environmental novelty, and abnormal social and emotion-related behaviors,[31] all known as hallmarks of the disease.

In fact, oligodendrocytes are highly vulnerable to altered redox state and oxidative stress. They display high metabolic activity and contain large stores of iron,[32] both of which favor ROS production. Despite that, they contain three times less GSH than astrocytes.[32] Oligodendrocytes and their progenitors are particularly sensitive to hydrogen peroxide[15] and nitric oxide inducers.[33] GSH deficit decreases the survival of oligodendrocyte progenitor cells (OPCs) *in vitro*.[34] In particular, pro-oxidants also modulate oligodendrocyte development.[35,36]

Table 1a. Demographic information for control subjects and early psychosis patients

(a) MRI study

	Control subjects (n = *40*)	*Patients* (n = *30*)	P-*value*
Age (years ± s.d.)	23.5 ± 3.2	23.1 ± 3.5	0.7[a]
Gender	25 men; 15 women	19 men; 11 women	1.0[b]
Antipsychotic medication (n)			
Quetiapine	NA	11	NA
Aripiprazole	NA	7	NA
Olanzapine	NA	4	NA
Amisulpride	NA	3	NA
Risperidone	NA	2	NA
Paliperidone	NA	1	NA
CPZ equivalent (mg ± s.d.)	NA	330.3[c] ± 218.9	NA
Psychosis duration (years ± s.d.)	NA	2.0 ± 1.8	NA

Abbreviations: CPZ, chlorpromazine equivalents; MRI, magnetic resonance imaging; n, number of individuals; NA, not applicable. [a]Independent two-tailed Student's *t*-test. [b]X^2 test. [c]Two patients without antipsychotic medication.

The notion that a redox dysregulation during critical periods of neurodevelopment could alter structural and functional connectivity has not yet been established. We propose that abnormal redox control could contribute to the white matter anomalies observed in schizophrenia. We thus hypothesized that GSH levels in the medial prefrontal cortex can be involved in the white matter integrity of the cingulum bundle, a fiber tract connecting frontal brain areas to posterior limbic structures. The finding of an association between prefrontal GSH levels and the cingulum white matter integrity in humans motivated us to study further the underlying mechanisms in experimental models. The consequences of a GSH deficit on OPCs and myelination during development were characterized using *in vitro* and *in vivo* models, including *GCLM*-KO mice.

MATERIALS AND METHODS

Subject recruitment

Patients in the early phase of psychosis, having met the threshold for psychosis (according to the CAARMS criteria)[37] were recruited from the TIPP Program (Treatment and Early Intervention in Psychosis Program, University Hospital, Lausanne, Switzerland).[38] Normal controls were recruited and assessed by the Diagnostic Interview for Genetic Studies.[39] Major mood, psychotic or substance-use disorder and having a first-degree relative with a psychotic disorder were the exclusion criteria for controls. At the time of magnetic resonance imaging (MRI) study, 28 patients were receiving antipsychotic medication, whereas 24 patients were receiving antipsychotic medication at the time of Fyn study (see Table 1a, Table 1b and Table 1c for details on demographic information, antipsychotic medication and chlorpromazine equivalent). Statistical analysis with one-way analysis of variance did not reveal any significant effect of chlorpromazine equivalents of antipsychotic drugs on GSH, Fyn mRNA and Fyn protein expression.

Diffusion and functional MRI acquisition and data processing

MRI was performed for all subjects on a 3 T scanner (Trio, Siemens Medical, Germany) with a 32-channel head coil. Diffusion spectrum imaging (DSI) was acquired and reconstructed as described in Wedeen *et al*.[40] Specifically, diffusion-weighted images were sampled in a Cartesian 3D grid of q-space using 128 diffusion-encoding gradients covering a hemisphere with *b*-values varying between 0 and 8000 s mm^{-2}. The acquisition volume was made of 96 × 96 × 34 voxels of 2.2 × 2.2 × 3 mm^3; TR/TE were, respectively, 6100/144 ms. Acquisition time was approximately 13 min. In addition, each subject was scanned in resting state conditions using a standard gradient echo planar imaging sequence sensitive to blood-oxygen-level-dependent contrast. An axial plane was used with a matrix of 64 × 58 voxels, each 3.3 × 3.3 mm^2. Thirty-two slices of 3.3 mm

Table 1b. Demographic information for control subjects and early psychosis patients

(b) Fyn mRNA study

	Control subjects (n = *15*)	*'GAG low-risk' patients* (n = *14*)	*'GAG high-risk' patients* (n = *14*)	P-*value*[a]
Age (years ± s.d.)	25.7 ± 6.3	23.0 ± 3.3	23.4 ± 3.4	0.23
Gender	15 men	14 men	14 men	NA
Antipsychotic medication (n)				
Quetiapine	NA	2	3	NA
Aripiprazole	NA	2	2	NA
Olanzapine	NA	4	2	NA
Amisulpride	NA	3	0	NA
Risperidone	NA	1	4	NA
Clozapine	NA	1	0	NA
CPZ equivalent (mg ± s.d.)	NA	358.4[b] ± 197.1	271.8[c] ± 149.9	NA

Abbreviations: ANOVA, analysis of variance; CPZ, chlorpromazine equivalents; n, number of individuals; NA, not applicable. [a]One-way ANOVA. [b]One patient without antipsychotic medication. [c]Three patients without antipsychotic medication.

Table 1c. Demographic information for control subjects and early psychosis patients

(c) Fyn protein study

	Control subjects (n = *12*)	*'GAG low-risk' patients* (n = *10*)	*'GAG high-risk' patients* (n = *10*)	P-*value*[a]
Age (years ± s.d.)	24.2 ± 3.1	23.0 ± 3.7	22.9 ± 2.8	0.57
Gender	12 men	10 men	10 men	NA
Antipsychotic medication (n)				
Quetiapine	NA	2	2	NA
Aripiprazole	NA	1	2	NA
Olanzapine	NA	3	1	NA
Amisulpride	NA	2	0	NA
Risperidone	NA	1	3	NA
Clozapine	NA	1	0	NA
CPZ equivalent (mg ± s.d.)	NA	361.0 ± 218.2	284.6[b] ± 200.7	NA

Abbreviations: ANOVA, analysis of variance; CPZ, chlorpromazine equivalents; n, number of individuals; NA, not applicable. [a]One-way ANOVA. [b]Two patients without antipsychotic medication.

thickness with a 0.3 mm gap were acquired. Repetition time was 1920 ms, and acquisition time was 9 min.

Furthermore, a magnetization-prepared rapid acquisition gradient echo sequence was acquired in a matrix of 240 × 256 × 160 voxels, 1 mm in-plane resolution and 1.2 mm slice thickness. TR/TI/TE were, respectively, 2300/900/2.98 ms. Acquisition time was approximately 4 min.

DSI, resting state functional MRI (fMRI) and magnetization-prepared rapid acquisition gradient echo data were processed using the Connectome Mapping Toolkit (http: //www.cmtk.org/)[41] and the Connectivity Decoding Toolkit,[42] as described below.

Generalized fractional anisotropy (gFA) in the cingulum bundle. (1) Gray and white matter were segmented from the magnetization-prepared rapid acquisition gradient echo acquisition, and the cortical surface was partitioned into 68 regions of interest with FreeSurfer software (http://surfer.nmr.mgh.harvard.edu/) according to the Desikan–Killiany atlas.[43] (2) Whole-brain streamline tractography was performed from the DSI using in-house software.[37] (3) Average gFA was extracted along the cingulum bundle defined as the connections between FreeSurfer regions: medial orbitofrontal, rostral anterior cingulate, caudal anterior cingulate, posterior cingulate, isthmus of cingulate and precuneus[44] (Figure 1a).

Functional connectivity along the cingulum bundle. (1) fMRI volumes were preprocessed including motion correction, regression of movement, average white matter and cerebrospinal fluid signals and linear detrending. (2) Resting state time series were averaged over the FreeSurfer cortical regions of interest, and band-pass filtered using the discrete wavelet transform.[42] (3) Functional correlation through the cingulum bundle was characterized with the Pearson's correlation between the average low-frequency cortical signals extracted from the medial prefrontal cortex (covering medial orbitofrontal and superior frontal cortex) on the one hand, and isthmus of the cingulate cortex and precuneus on the other hand (Figure 1a).

MRS and data processing

For each individual, MRS experiment was assessed the same day than diffusion and functional MRI with a time interval of 30 min between the acquisitions. All MRS experiments were performed with a transverse electromagnetic volume head coil (MR Instruments, Minneapolis, MN, USA). The magnetic field homogeneity was optimized by adjusting first- and second-order shims using FAST(EST)MAP.[45] *In vivo* proton nuclear magnetic resonance spectra were acquired from a volume of interest positioned in the medial bilateral prefrontal lobe using short-TE spin-echo full-intensity acquired localized single voxel spectroscopy technique.[46,47] The following scan parameters were used: volume of interest = 20 × 20 × 25 mm^3, TR/TE = 4000/6 ms, acquisition bandwidth = 2 kHz, number of averaged = 148 and vector size = 2048. GSH concentration was obtained by analyzing water-suppressed *in vivo* proton nuclear magnetic resonance spectra using LCModel[48] with a basis set consisting of simulated individual metabolite spectra (Supplementary Figure 1).[49] Unsuppressed water proton nuclear magnetic resonance spectra were used as an internal reference for the quantification of metabolite concentrations. The spectral range for analysis was set to 0.2–4.2 p.p.m. By using the short-TE MRS technique at 3T, GSH was quantified with a Cramer–Rao lower bounds of 7 ± 2% (mean ± s.d.).

Fibroblast cell culture and treatment

Fibroblast cell cultures were obtained from skin biopsies using a standard procedure.[22] Cells were grown in Dulbecco's modified Eagle's medium (DMEM) supplemented with 2% Ultroser-G serum (Biosepra, Cergy, France), 1 mM sodium pyruvate, 100 U ml^{-1} penicillin and 100 μg ml^{-1} streptomycin. Fibroblasts were plated at 73 cells per mm^2. One day after plating, we treated fibroblasts with 50 μM *tert*-butylhydroquinone (tBHQ) or vehicle for 18 h. Cells were trypsinized, pelleted and stored at − 80 °C.

Animals

GCLM-KO mice generated by Yang *et al.*[50] were bred, weaned, genotyped and maintained as described previously.[31] All animal procedures were approved by the Swiss cantonal veterinary office.

Oligodendroglial cell culture and lentivirus infection

Mixed glial primary cell cultures were prepared from 1- to 3-day-old Wistar rat. Cerebral cortices were dissected and dissociated in papain solution (20 U ml^{-1} papain, 100 U ml^{-1} DNase and 1 mM L-cysteine in L15 medium) for 30 min at 37 °C, followed by mechanic dissociations. Cells derived from one brain were grown into two poly-L-ornithine-coated 75 cm^2 flasks in DMEM with 10% fetal calf serum and 100 U ml^{-1} penicillin–100 μg ml^{-1} streptomycin. After 7 days, one flask was transduced with lentivirus containing the scrambled short hairpin RNA (shRNA) and the other with GCLC shRNA (multiplicity of infection of 5). Puromycin (1 μg ml^{-1}) was added 2 days after cell transduction for 24 h. This puromycin dose and time of treatment were normally toxic for non-transduced oligodendrocyte cells. Transduction efficiency was estimated to be > 95%. OPCs were then isolated by a method adapted from McCarthy and de Vellis.[51] Briefly, flasks were shaken for 1 h at 37 °C, rinsed two times with DMEM and shaken for 18 h at 37 °C. The supernatant was plated in a plastic dish for 45 min, and then OPCs (supernatants) were plated in poly-L-ornithine-coated coverslips and maintained in DMEM medium supplemented with 100 U ml^{-1} penicillin–100 μg ml^{-1} streptomycin, 2.5 μM forskolin, 50 μg ml^{-1} apo-transferrin, 5 μg ml^{-1} insulin, 30 nM sodium selenate, 10 nM hydrocortisone, 10 nM D-biotin, 1 mg ml^{-1} bovine serum albumin, 10 ng ml^{-1} platelet-derived growth factor-AA (PDGF-AA) and 10 ng ml^{-1} basic fibroblast growth factor (bFGF). In late differentiation experiments, OPCs were grown in medium lacking growth factors (PDGF-AA and bFGF) and supplemented with 40 ng ml^{-1} 3,3′,5-triiodo-L-thyronine (thyroid hormone: T3) from 7 days after transduction. OPCs were exposed to 1 mM of *N*-acetylcysteine (NAC; Sigma, St Louis, MO, USA), or 1 μM 4-amino-5-(methylphenyl)-7-(t-butyl)pyrazolo-(3,4-d)pyrimidine (PP1) (Fyn inhibitor; Sigma), or to vehicle for 24 h.

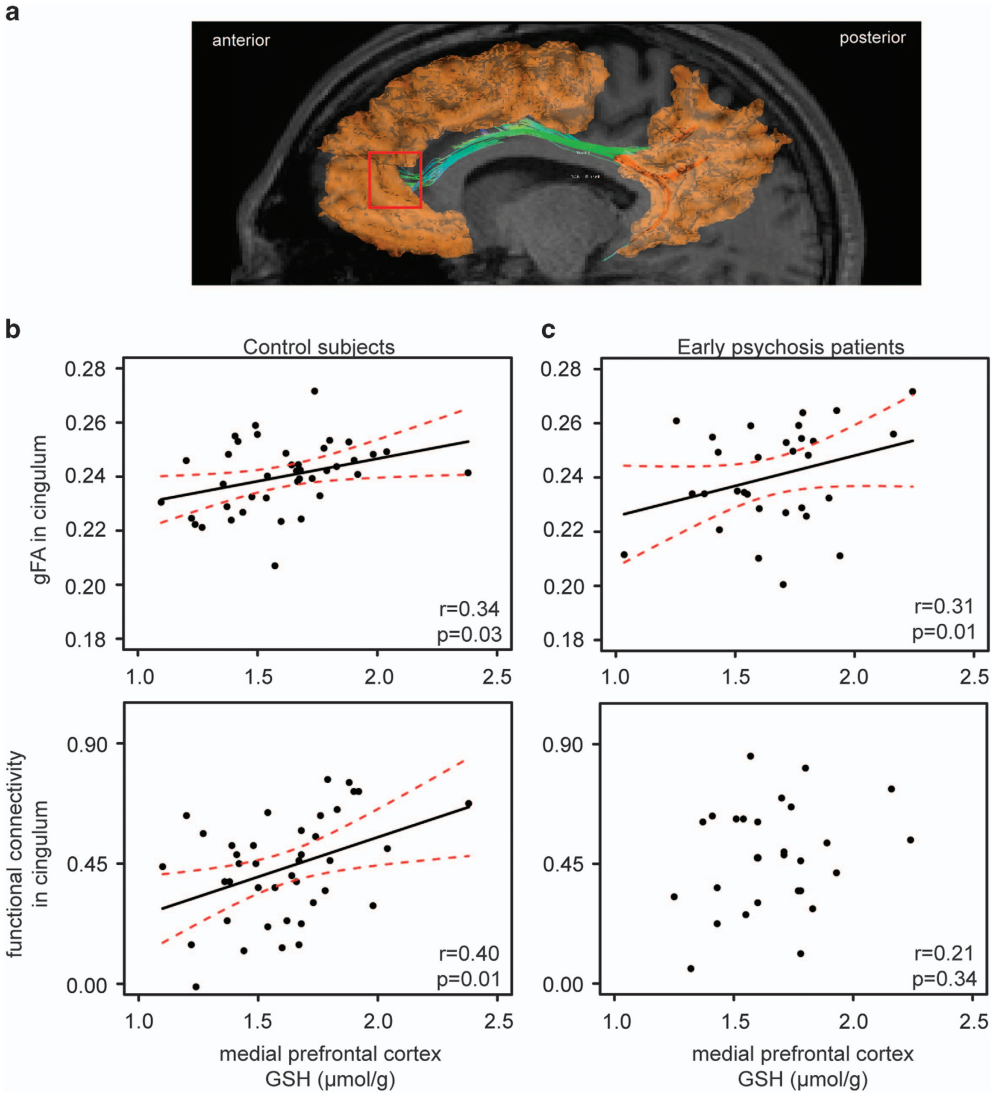

Figure 1. Association between glutathione (GSH) levels in the medial prefrontal cortex and white matter integrity (generalized fractional anisotropy (gFA)) and functional connectivity along the human cingulum bundle. (**a**) Representation of the cingulum bundle in green, illustrating the white matter tract along which the gFA values have been averaged. Red box indicates the volume of interest used for GSH level measurement. The cingulate cortical regions considered for the evaluation of the functional connectivity through the cingulum are represented in orange, and include the medial prefrontal cortex, the isthmus of the cingulate cortex and the precuneus. (**b** and **c**) Scatter plots of medial prefrontal GSH levels and both gFA values (top panels) and functional connectivity (bottom panels) along the cingulum bundle in control subjects (**b**) and early psychosis patients (**c**). Each point in the scatter plots represents one subject and red lines represent the confidence intervals. $*P < 0.05$ with Pearson's correlation and generalized additive model.

Antibodies

Antibodies used for immunofluorescent staining were as follows: rabbit polyclonal anti-NG2 (1:600; Millipore, Temecula, CA, USA), mouse monoclonal anti-O4 (1:200; Millipore), mouse monoclonal anti-2′,3′-cyclic-nucleotide 3'-phosphodiesterase (CNP) (1:500, clone 11-5B; Chemicon, Temecula, CA, USA), rat monoclonal anti-myelin basic protein (MBP) (1:400; Millipore), mouse monoclonal anti-APC (CC1; 1:70; Calbiochem, San Diego, CA, USA), rabbit polyclonal anti-PDGF receptor (PDGFR) (1:350; Santa Cruz, Santa Cruz, CA, USA), mouse anti-bromodeoxyuridine (BrdU) (Roche Applied Science, Mannheim, Germany), Cy3 goat anti-mouse IgG (1:300; Molecular Probes, Eugene, OR, USA), Alexa 488 goat anti-rabbit IgG or anti-mouse IgG (1:300; Molecular Probes), Cy3 goat anti-rat IgG (1:600; Millipore) and anti-mouse-Ig-fluorescein (Roche Applied Science). For western blot experiments, we used mouse antibody to GCLC at 1:10 000 (kindly provided by P Vliet, University of Washington, Seattle, WA, USA), rabbit polyclonal anti-PDGFR (1:2000; Santa Cruz), mouse monoclonal anti-Fyn (1:1000; Abcam, Cambridge, UK), mouse monoclonal anti-CNP (1:2000; clone 11-5B; Chemicon), mouse monoclonal anti-α-tubulin (1:200; Santa Cruz), mouse monoclonal anti-β-actin (1:10 000; Abcam) and horseradish peroxidase-conjugated anti-mouse or anti-rabbit (1:10 000; GE Healthcare, Buckinghamshire, UK). Mouse monoclonal antibody to Fyn (Abcam) was used to immunoprecipitate Fyn kinase protein.

Immunohistochemistry, confocal microscopy and image analysis

Forty- and 90-day-old *GCLM*-KO mice or wild-type mice were anesthetized, perfused and their brains were removed as described in Cabungcal *et al.*[52] Briefly, three to six consecutive sections (40 μm) from each animal (bregma 1.14–1.34 mm) were selected, permeabilized with 0.3% Triton X-100 in 0.1 M phosphate-buffered saline (PBS) and blocked for 1 h in 0.1 M PBS, 0.3% Triton X-100 and 2% normal goat serum. Sections were incubated for 48 h at 4 °C with the primary antibodies diluted in blocking buffer. After incubation with secondary antibodies in 0.1 M PBS, 0.3% Triton X-100 for 1 h at room temperature (RT), sections were counterstained with DAPI (4′-6-diamidino-2-phenylindole: 1.5 μM in 0.1 M PBS; Molecular Probes) for 10 min, and were mounted in Mowiol solution. Based on the anatomical

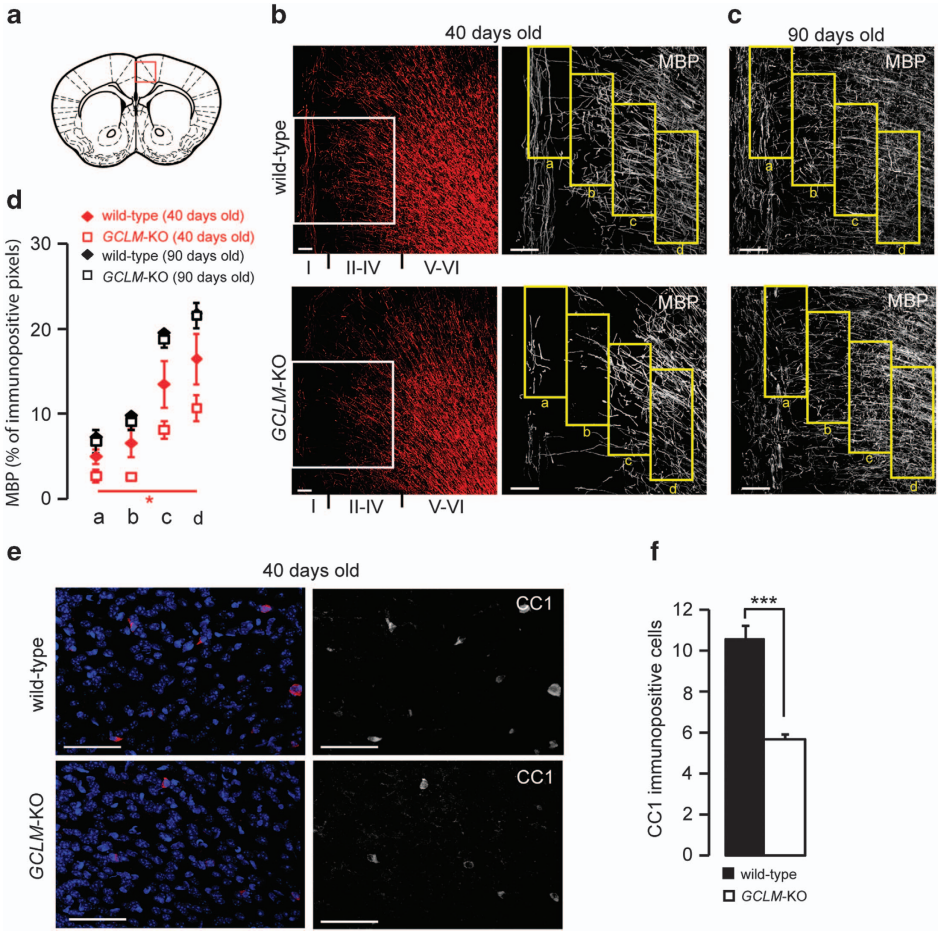

Figure 2. Forty-day-old *GCLM*-KO mice present a decreased immunoreactivity for the myelin-associated protein MBP and the mature oligodendrocyte marker CC1 in the anterior cingulate cortex. (**a**) Schematic drawing of coronal section with anterior cingulate cortex included in the red square, illustrating the region analyzed in panels **b**–**d**. (**b** and **c**) Confocal images showing MBP labeling in wild-type and *GCLM*-KO mice. White boxes represent the region shown in the magnified images in which four different areas (yellow boxes) of 0.02 mm^2 were placed from layer I, and used to quantify MBP labeling in mice, at 40 (**b**) and 90 days old (**c**). Scale bar: 50 μm. (**d**) Quantification of MBP-positive pixels in each delimited area for wild-type (diamond) and *GCLM*-KO (square) mice, at 40 (red) and 90 days old (black) ($n = 6$–8 animals per group). Data are expressed as mean ± s.e.m. $^*P < 0.05$, analyzed by linear mixed-effect model. (**e**) Confocal images showing mature oligodendrocytes labeled with CC1. Scale bar: 50 μm. (**f**) Quantification of CC1-positive cells in area of 0.08 mm^2 including layers I–IV ($n = 6$ animals per group). Data are expressed as mean ± s.e.m. $^{***}P < 0.001$, analyzed by Student's *t*-test. GCLM, gene coding for the modifier subunit of the glutamate-cysteine ligase; KO, knockout; MBP, myelin basic protein.

cytoarchitectonic areas given by Franklin and Paxinos,[53] the anterior cingulate cortex (bregma ~ 1.14–1.34) was delineated from the boundaries of infralimbic and secondary motor cortices, including the cingulate cortex area 1 (cg1) and part of area 2 (cg2).[30] Images were captured with Zeiss LSM 710 Quasar confocal microscope equipped with a x40 objective (Zeiss, Göttingen, Germany). Z-stack of 10 images was scanned. As fiber labeling with MBP and CNP was dense, the first five and last five images of the z-stack were treated separately. Images were reconstituted with Imaris 6.2 software (Bitplane, Zürich, Switzerland). In ImageJ (National Institutes of Health, Bethesda, MD, USA), four areas of 0.02 mm^2 were placed from layer I (Figure 2b). For MBP and CNP quantification, a fixed intensity threshold was applied in each area and ratio of stained pixels over the total pixel number was calculated. Each value for one area corresponds to the mean of sum of both z-stack groups. For CC1 or PDGFR labeling, a fixed intensity threshold was applied in each area and the number of CC1- or PDGFR-positive cells over 60 pixels was quantified. Values reported correspond to the sum of CC1- or PDGFR-positive cells in all areas.

shRNA construction and lentivirus particle production

GCLM shRNA (5′-CTCAGTCCTTGGAGTTGCAttcaagagaTGCAACTCCAAGGACTGAG-3′), GCLC shRNA (5′-GGAGGCTACTTCTATATTAttcaagagaTAATATAGAAGTAGCCTCC-3′) and scramble shRNA (5′-CTTACAATCAGACTGGCGAttcaagagaTCGCCAGTCTGATTGTAAG-3′) were inserted in a pSP-93 P vector containing puromycin resistance gene (the nucleotides of the shRNA loop are indicated by lowercase letters).

Human embryonic kidney 293 T cells were plated and transfected the day after using calcium phosphate method with the vectors coding for virion packaging elements (5 μg pMD2.G; 15 μg pCMV-dR8.74) and vector genome (20 μg shRNA-pSP-93 P). The medium was replaced 8 h after transfection. Supernatants were collected 24 h later, filtered through 0.45 μm membrane, pelleted at 19 000 r.p.m. for 90 min at 4 °C and resuspended in DMEM. Lentivirus titration was measured with HIV-1 p24 antigen ELISA Kit (ZeptoMetrix, Buffalo, NY, USA).

Monochlorobimane assay

Cells were incubated with 100 μM monochlorobimane (Sigma) in HEPES buffer (140 mM NaCl, 5 mM KCl, 20 mM glucose, 2 mM $CaCl_2$, 10 mM HEPES, 1 mM $MgCl_2$, pH 7.4) and fluorescence emission (460 nm) was measured every minute for 40 min under inverted Nikon Eclipse TE300 microscope equipped with a x20 objective (Nikon, Küsnacht, Switzerland). For quantification in MetaMorph, we selected image captured at 40 min and we subtracted the background. Each value reported corresponds to mean fluorescence intensity of cells.

Survival assay

Sytox Orange Nucleic Acid Stain (Invitrogen, Eugene, OR, USA) was added to cells at 1 μM for 30 min at 37 °C before fixation. Nuclei were labeled with DAPI for 10 min and coverslips were mounted in Mowiol solution. Four images per coverslip were captured with Axioskop2 fluorescence microscope equipped with a x16 objective (Zeiss). We calculated ratio between Sytox-positive cell number and total cell number with ImageJ. Values reported correspond to the mean of ratio from the four images.

Proliferation assay

OPCs were treated with 10 μM BrdU (Roche Applied Science) for 4 h at 37 °C. Cells were fixed, blocked (2% normal goat serum in PBS for 30 min) and immunolabeled following the manufacturer's instructions. After DAPI staining, coverslips were mounted in Mowiol solution. Images were captured using Axioskop2 fluorescence microscope equipped with a x16 objective (Zeiss). We analyzed four images per condition with ImageJ. Values reported represent the mean of ratio between BrdU- and NG2-positive cells.

Immunocytochemistry and quantification

After fixation, cells were permeabilized with 0.1% Triton X-100 in PBS for 5 min at RT, and blocked in 0.1 M PBS, 2% normal goat serum and 0.1% Triton X-100 for 30 min at RT. Primary antibodies were incubated in PBS, 2% normal goat serum, 0.1% Triton X-100 for 30 min at 37 °C. After incubation with secondary antibodies in PBS for 30 min at 37 °C, cells were counterstained with DAPI for 10 min. Coverslips were mounted in Mowiol solution. Four images per coverslip were captured with Axioskop2 fluorescence microscope equipped with a x40 objective (Zeiss). On each image, we quantified the ratio between immunopositive cells and total cell number using ImageJ.

Western blot

Anterior cingulate cortex from mice was incubated for 10 min on ice in extraction buffer (50 mM Tris-HCl (pH 7.5), 250 mM NaCl, 1% sodium dodecyl sulfate, 1 mM dithiothreitol, 1 mM EDTA, 0.01% phenylmethanesulfonyl fluoride and protease inhibitor cocktail; Roche, Mannheim, Germany), sonicated and centrifuged 15 min at 10 000 *g*. OPC pellets were incubated for 10 min in RIPA buffer on ice and centrifuged 15 min at 10 000 *g*. Fibroblast pellets were suspended in ice-cold lysis buffer (50 mM Tris-HCl (pH 7.5), 150 mM NaCl, 1 mM EDTA, 1% Triton, 0.1% sodium dodecyl sulfate, 30 mM sodium fluoride, 1 mM phenylmethanesulfonyl fluoride, 30 mM β-glycerophosphate, 0.2 mM sodium orthovanadate and protease inhibitor cocktail; Roche) and centrifuged 15 min at 10 000 *g*. Proteins were separated by sodium dodecyl sulfate-polyacrylamide gel electrophoresis on 10% acrylamide gels, and transferred on PVDF membrane (Millipore). After blocking in Tris-buffered saline (TBS), 0.1% Tween-20 (TBST), 5% milk for 1 h at RT, membranes were incubated overnight at 4 °C with primary antibodies diluted in TBST and 3% bovine serum albumin. Membranes were incubated with horseradish peroxidase-conjugated secondary antibody in TBST and 0.5% milk for 1 h at RT. Peroxidase activities were detected using Amersham ECL Kit (GE Healthcare). Positive signal was analyzed and normalized to α-tubulin or β-actin with ImageJ.

Immunoprecipitation and Fyn kinase activity

Cell lysates (150 μg) were precleared by incubation with Dynabeads Protein G (Invitrogen) 30 min at 4 °C, before hybridization with 6 μg of Fyn antibody for 1 h at RT. Complexes were pulled down with 50 μl Dynabeads Protein G for 30 min at RT. After immunoprecipitation, Fyn activity was measured according to the manufacturer's protocol (Universal Tyrosine Kinase Assay Kit; Takara, Shiga, Japan).

RNA isolation and qRT-PCR

RNA were extracted using PerfectPure RNA cultured cell Kit (5Prime, Hamburg, Germany) or AllPrep DNA/RNA/Protein Mini Kit (Qiagen, Hilden, Germany) as described in the manufacturer's protocol. As indicated by the absorbance ratio 260/280 nm (human samples: 2.08 ± 0.01; animal model samples: 2.01 ± 0.02; culture samples: 2.10 ± 0.01), RNA were accepted as pure RNA. cDNA were synthesized using the following reaction mix: 300 ng RNA, 5.5 mM $MgCl_2$, 2 mM dNTP, 0.4 U μl^{-1} RNasin inhibitor, 2.5 μM random hexamer, 1.25 U μl^{-1} RTase and bufferRT 10x from Applied Biosystem. Taqman real-time PCR was performed in a final volume of 20 μl containing 10 ng cDNA, and 1 μl of selected probes mixed with 10 μl of TaqMan Universal PCR Master Mix (Applied Biosystems). Probes used were as follows: 18S (4333760 T), Fyn (Hs00941600_m1), p27kip1 (Rn00582195_m1), cyclin D1 (Rn00432360_m1), Rpl27 (Rn00821099_g1), β-tubulin (Mm00495806_g) and Fyn (Ms00433373_m1). Quantitative PCR was performed on Applied Biosystems 7500 Fast Real-Time PCR System and the 7500 Fast System SDS Software as established by the provider (Applied Biosystems, Foster City, CA, USA). Samples were run in duplicate. In the animal model, data were normalized to the internal control β-tubulin and a cerebellum sample. In OPC cultures, data were normalized to mean between internal control 18S and Rpl27. To prevent amplification fluctuation of the housekeeping gene *GAPDH* in response to tBHQ treatment, we normalized human data with 18S, a more stable control gene. Data were analyzed using ΔΔCt method.[54]

Statistical analysis

Statistics were performed with R version 2.13. Data from MBP and CNP immunohistochemistry were analyzed by linear mixed-effect model. *In vitro* and *in vivo* data that followed a normal distribution (verified by Shapiro test) were analyzed by paired Student's *t*-test. Otherwise, a nonparametric test (Wilcoxon's test) was applied. For multiple comparisons (control vs NAC or dimethyl sulfoxide (DMSO) vs PP1), we used a linear mixed-effect model. Antipsychotic drug effect on GSH and Fyn was analyzed with analysis of variance. Pearson's correlation was used to study the relationship between GSH and both gFA and functional connectivity in control subjects. In early psychosis patients, we noticed highly nonlinear relations between psychosis duration, medication dose and both gFA and functional connectivity. Consequently, generalized additive model was used to measure the association between GSH and both gFA and functional connectivity, allowing a smooth semiparametric relation between explanatory and response variables without imposing any parametric relation on the model.

RESULTS

Relationship between frontal GSH levels and connectivity in the human cingulum bundle

In control subjects and early psychosis patients, we investigated the relationship between medial prefrontal GSH levels, measured by proton magnetic resonance spectroscopy, and white matter integrity in the cingulum bundle, assessed with DSI and the derived gFA values (Figure 1a).[40] In addition, the functional connectivity along the cingulum (between the medial prefrontal cortex on one side and the isthmus of the cingulate cortex and precuneus on the other) was assessed with resting state fMRI (Figure 1a).[55] To focus on the prefrontal maturation period, we included only individuals younger than 30 years old;[56] controls and patients were matched for age and gender (Table 1a). In control subjects, significant positive correlations between GSH levels and both gFA values and the functional connectivity along the cingulum were found ($r = 0.34$, $P = 0.03$/$r = 0.40$, $P = 0.01$) (Figure 1b). In early psychosis patients, GSH levels were also positively associated with gFA values when medication and psychosis duration were included as covariates ($r = 0.31$, $P = 0.01$), while functional connectivity did not show any correlation with GSH levels even including these cofactors ($r = 0.21$, $P = 0.34$) (Figure 1c). These findings indicate a potential dependence between GSH levels and white matter integrity during the prefrontal cortex development in control subjects and patients. Moreover, GSH levels are associated with the functional connectivity in control subjects, a mechanism likely disrupted in schizophrenia.

GSH deficit affects oligodendrocyte maturation and myelination

To explore the influence of brain GSH levels on myelination in the prefrontal cortex (in particular, anterior cingulate cortex; Figure 2a), we used a mouse model that has low GSH levels (*GCLM*-KO). The immunolabeling for two myelin-associated proteins, CNP and MBP, was decreased in *GCLM*-KO mice as

compared with wild-type animals at peripubertal age (CNP: $P=0.03$; MBP: $P=0.01$) (Figures 2b and d and Supplementary Figures 2a and c) but not in adulthood (Figures 2c and d and Supplementary Figures 2b and c). Quantification revealed a reduction of MBP immunostaining from the superficial layer to deeper layers in peripubertal *GCLM*-KO mice compared with wild-type mice: $45\pm15\%$ in area a, $63\pm5\%$ in area b, $41\pm7\%$ in area c and $35\pm9\%$ in area d (Figure 2d). Similar results were obtained with CNP immunolabeling ($39\pm15.3\%$, $62\pm6.1\%$, $43\pm3.9\%$, $40\pm9.1\%$ for areas a–d, respectively) (Supplementary Figure 2c). We also quantified the number of OPCs labeled with PDGFR marker and the number of mature oligodendrocytes labeled with CC1 marker. At peripubertal stage, the level of PDGFR-positive cells was similar in wild-type and *GCLM*-KO mice (Supplementary Figures 2d and e). However, the number of CC1-positive cells was reduced by $46.1\pm2.5\%$ in the anterior cingulate cortex of *GCLM*-KO mice ($P=0.0005$) (Figures 2e and f). These observations indicate a critical role of GSH levels for oligodendrocyte maturation that affects myelin formation during the peripubertal period.

GSH synthesis deficit impairs proliferation and maturation of OPC

To further investigate the mechanism underlying the effect of redox dysregulation on oligodendrocyte maturation, we used OPC-enriched primary cultures ($94\pm0.4\%$ NG2-positive cells) to assess proliferation and differentiation of OPCs having lower GSH levels (Figure 3a). Deficit in intracellular GSH was induced by transducing cells with lentiviral particles containing an shRNA targeting the catalytic or modulatory subunit of GCL, the rate-limiting enzyme of GSH synthesis. At 7 days after infection, the GCLC shRNA caused a $49\pm5\%$ reduction in GCLC subunit as shown by western blot ($P=0.005$) (Figure 3b) and a $28\pm8\%$ decrease in GSH levels compared with control cells transduced with scrambled sequence shRNA ($P=0.02$) (Figure 3c). The GSH decrease induced with GCLC shRNA remained stable for at least 10 days ($P=0.009$) (Figure 3c). In contrast, GCLM shRNA reduced GSH levels only by $15\pm11\%$ (data not shown) and thus was not further used. Proliferation of OPCs was evaluated by BrdU incorporation at 7 days after infection (Figure 3d). The double staining with BrdU and NG2 indicated that GCLC shRNA led to a $29\pm7\%$ reduction in OPC proliferation as compared with scrambled shRNA ($P=0.004$) (Figure 3e). In addition, to evaluate the consequence of GSH deficit on cell cycle, we measured mRNA expression of p27kip1, an inhibitor of cell cycle, and cyclin D1, a positive marker for cell cycle progression. No significant difference in p27kip1 expression levels was found between GCLC shRNA samples as compared with scrambled conditions ($P=0.16$) (Supplementary Figure 3a). However, quantification of cyclin D1 indicated a reduction of $19\pm7\%$ in GCLC shRNA conditions as compared with scrambled shRNA ($P=0.05$) (Supplementary Figure 3a). To determine if the effect was due to an increase in cell death, we assessed necrosis and apoptosis levels by using Sytox dye. The percentage of Sytox-positive cells was low and homogenous among groups. In scrambled conditions, $0.7\pm0.2\%$ of cells were Sytox positive and $0.8\pm0.3\%$ were labeled with Sytox in GCLC shRNA conditions (Supplementary Figures 3b and c). This indicates that a 28% GSH decrease did not affect OPC survival. NAC, a redox regulator and GSH precursor, prevented the decrease of proliferation induced by GSH deficit in GCLC shRNA conditions (Figure 3e), but also increased OPC proliferation by a factor of 1.7 ± 0.4 (Figure 3e).

Early differentiation of the progenitor cells occurring without exogenous differentiation factors (thyroid hormone: T3) was also assessed by immunocytolabeling of stage-specific markers: O4 for preoligodendrocytes and CNP for oligodendrocytes (Supplementary Figure 4). At 7 days after infection, the density of O4- or CNP-positive cells was similar in cells transduced with GCLC or control shRNA (Figure 3f). However, at 10 days after infection, the proportion of O4- and CNP-positive cells was, respectively, 1.7 ± 0.2 and 2.7 ± 0.3 times higher in conditions with GCLC shRNA than with the control shRNA (O4: $P=0.05$; CNP: $P=0.002$) (Figure 3g). Taken together, this indicates that a GSH deficit may promote the switch from proliferation to early differentiation.

To evaluate the consequence of GSH deficit on a more mature oligodendrocyte stage, we cultured OPCs with exogenous differentiation factors (T3) from 7 days after infection. The level of CNP protein expression in control and GCLC shRNA OPC cultures was, respectively, 2.7 ± 0.4 times higher in the differentiating medium (T3) than in the proliferating medium (PDGF-AA, bFGF) ($P=0.005$) (Figure 3h). However, the number of mature oligodendrocyte labeled with MBP was reduced by $57.2\pm11\%$ in GSH-deficit conditions ($P=0.01$) (Figures 3i and j).

These observations suggest that a compromised GSH synthesis decreases proliferation, increases early differentiation of OPCs but impairs oligodendrocyte maturation in a later stage. We then explored the molecular mechanism that could link GSH deficit to the impairment in oligodendrocyte maturation processes.

GSH synthesis deficit affects Fyn kinase

It has been suggested that OPC proliferation may depend on PDGFR-mediated pathway and the switch from proliferation to early differentiation is in part due to a Fyn kinase-mediated degradation of PDGFR.[57,58] Therefore, we asked whether an upregulation of Fyn was responsible for the decreased proliferation in OPCs transduced with GCLC shRNA. At 7 days after infection, the levels of PDGFR protein expression were reduced by $16\pm5\%$ in GCLC shRNA compared with scrambled shRNA OPC cultures ($P=0.03$) (Figure 4a). While there was no difference in Fyn protein levels between control and GCLC shRNA OPCs (Figure 4b), a twofold increase in Fyn kinase activity was observed under GSH-deficit conditions ($P=0.04$) (Figure 4c). Inhibition of Fyn with PP1 prevented the decreased proliferation of OPCs induced by GCLC shRNA ($P=0.02$) (Figure 4d). These *in vitro* results indicate that a GSH deficit leads to a reduction of OPC proliferation through an increase of Fyn kinase activity that likely decreases PDGFR protein levels.

Then, we investigated whether an Fyn upregulation was also present in the anterior cingulate cortex of *GCLM*-KO mice. Fyn mRNA expression was increased by 1.2 ± 0.05 times in 20-day-old but not 40- and 90-day-old *GCLM*-KO mice as compared with age-matched wild-type mice ($P=0.04$) (Figure 4e). Consistently, Fyn protein levels were also increased by 1.2 ± 0.05 times in 20-day-old *GCLM*-KO mice as compared with wild-type mice ($P=0.007$) (Figure 4f). These indicate that Fyn is upregulated during the development of prefrontal cortex in animal model with low GSH levels.

Abnormal Fyn mRNA and protein expression in early psychosis patient with redox impairments

We then assessed whether abnormal Fyn kinase levels were also found in early psychosis patients with a redox dysregulation. We investigated Fyn regulation in response to oxidative stress induced by *tert*-butylhydroquinone (tBHQ) in skin-derived fibroblasts. In a previous study, we found that under oxidative stress conditions, GSH levels were significantly lower in fibroblasts with 'GAG high-risk' compared with 'GAG low-risk' GCLC genotypes.[20] This and another study on plasma thiol levels indicate that the 'GAG high-risk' is associated with impaired redox regulation.[28] Here, we compared Fyn mRNA expression in fibroblasts from control subjects ('GAG low-risk') with that of early psychosis patients ('GAG low-risk' and 'GAG high-risk' genotypes) (Table 1b). In absence of tBHQ, Fyn mRNA levels were homogeneous in all three groups (Figure 4g). The oxidative challenge led to Fyn mRNA downregulation in fibroblasts from control subjects and 'GAG low-risk' patients, as compared with vehicle treatments ('GAG low-risk' control subjects: $P=0.007$; 'GAG low-risk' patients: $P=0.01$) (Figure 4h). In contrast, no such downregulation was observed in fibroblasts of 'GAG high-risk' genotypes associated with low GSH levels (Figure 4h). Likewise, Fyn protein levels were

downregulated in fibroblasts from control subjects and 'GAG low-risk' patients in response to tBHQ treatment ('GAG low-risk' control subjects: $P = 3.6e^{-06}$; 'GAG low-risk' patients: $P = 0.02$) (Figure 4i). However, in fibroblasts of 'GAG high-risk' genotypes, Fyn protein expression was not different in response to oxidative stress (Figure 4i). In conclusion, fibroblasts from schizophrenia patients with a genetic risk for an abnormal redox regulation also display an impaired regulation of Fyn mRNA and protein expressions.

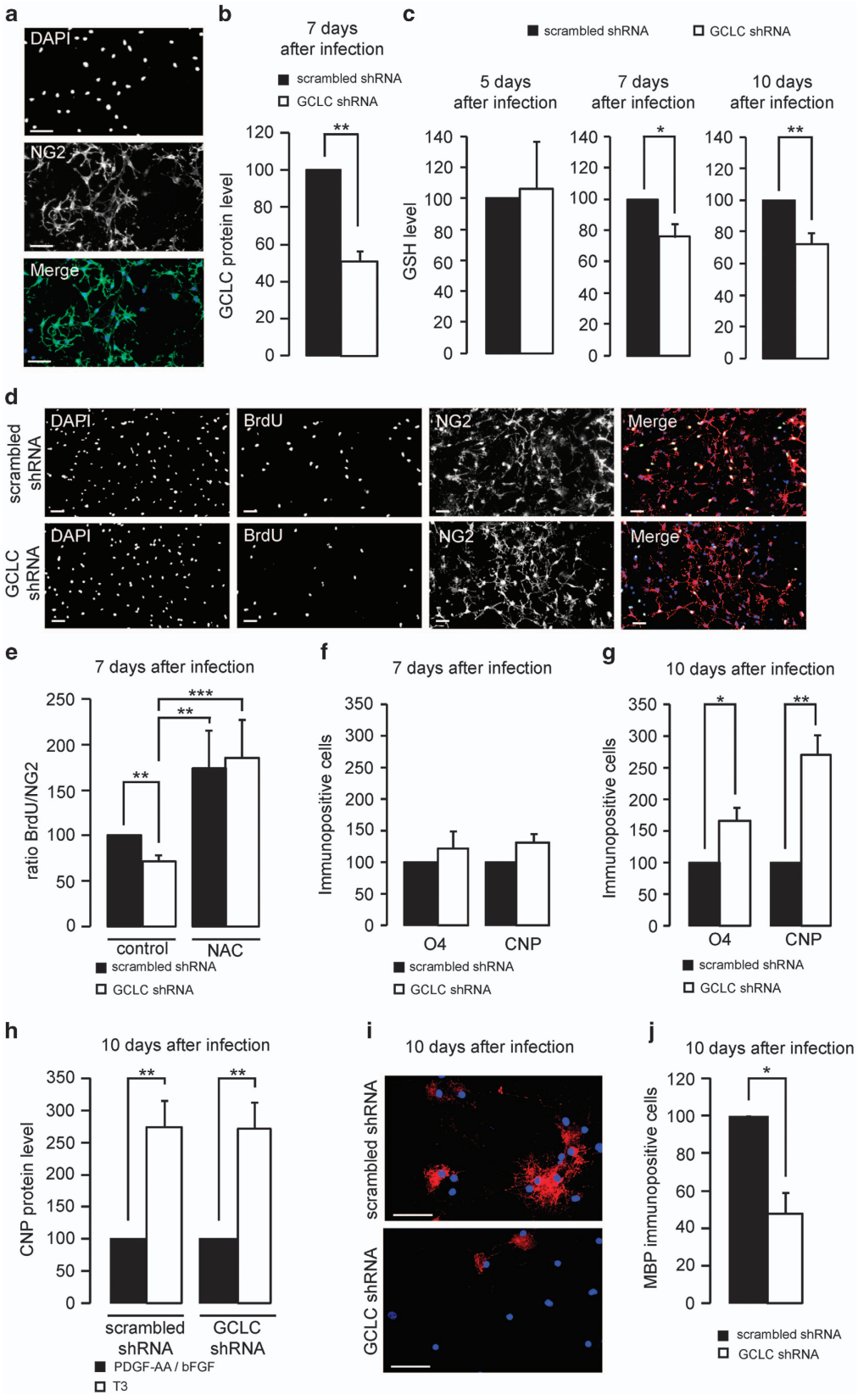

DISCUSSION

The present study highlights an important role of GSH for oligodendrocyte differentiation and myelination processes. We found that GSH levels measured in the medial prefrontal cortex are positively associated with white matter integrity in the cingulum bundle of young healthy subjects and early psychosis patients. In the anterior cingulate cortex of peripubertal *GCLM*-KO mice, a constitutive GSH deficit causes reduced expression of myelin-associated proteins and decreased number of mature oligodendrocytes. Using OPC cultures, we found that a deficit in GSH decreases OPC proliferation via Fyn upregulation, and it also impairs oligodendrocyte maturation. Consistently, fibroblasts of patients carrying 'GAG high-risk' genotypes in the *GCLC* gene, which are associated with a phenotype of compromised GSH synthesis and redox dysregulation, present abnormal regulation of Fyn when challenged with an oxidative stress.

Our observation that a GSH deficit decreases OPC proliferation and promotes early differentiation is in agreement with previous studies showing a switch from OPC division to early differentiation following treatment with either buthionine sulfoximine (BSO), an inhibitor of GSH synthesis, or pro-oxidants (i.e. methylmercury, lead, paraquat) in the absence of differentiating factors in the medium.[57,58] However, when differentiating factors are added to the medium, a deficit in GSH induced either by GCLC shRNA (this study) or BSO[59] impairs oligodendrocyte maturation. These latter *in vitro* data are consistent with the impaired oligodendrocyte and myelination observed in *GCLM*-KO mice. Moreover, these data are further supported by the positive relationship between GSH levels and gFA along the cingulum bundle in young healthy subjects and early psychosis patients. This suggests a role for GSH during the development of fibers, either at the level of myelin or axonal size or fiber packing since gFA can be influenced by these various factors.[60] Taken together, these suggest that a proper timing of redox regulation and differentiation signals is crucial to control the proliferation and the various stages of oligodendrocyte differentiation. Thus, abnormal control of redox system could therefore affect myelination processes and white matter integrity along various developmental periods.

Myelination of the prefrontal lobe progresses through adolescence and completes only in early adulthood.[61–63] Although the dynamics of this process may be different in rodents, our observation that *GCLM*-KO mice present a myelin deficit in the anterior cingulate cortex during peripubertal period and no myelin impairment at adulthood suggests that this latter is a vulnerable time period during which an adequate redox control is required. In agreement with this interpretation, a transcriptomic study in the prefrontal cortex identified genes for which expression profiles specifically peak during late adolescence through early adulthood (i.e. between ages 15 and 25 years). Besides genes related to either myelin or lipid synthesis, the antioxidant response system is one of the most highly expressed during this period.[62] In line with this, we found a positive association between GSH levels and gFA only when individuals under 30 years of age were included. This corresponds to an age until which the cingulum bundle is still maturing.[56] Early adulthood coincides with the mean onset of schizophrenia and the development of higher cognitive processes such as executive function and social cognitive function,[64] both of which are affected in the disease. We propose that abnormal redox control during the period of myelin maturation could lead to disrupted connectivity in the prefrontal cortex and contribute later in the appearance of the symptoms. Moreover, oligodendrocyte and myelin impairments may be implicated in cognitive dysfunction.[65,66]

In control subjects, GSH levels also positively correlate with the functional connectivity between the medial prefrontal and the posterior cingulate cortices in control subjects. Therefore, higher GSH levels correspond to better synchronization of these two areas, in line with their higher gFA values.

In the current study, no significant difference in prefrontal GSH levels was observed between patients and control subjects. It should be noted that the MRS/MRI was performed under 'resting' conditions. Indeed, in a previous study with patient-derived fibroblasts, all patients showed a compromised upregulation of antioxidant defense as compared with control subjects only under conditions of challenge by oxidative stress.[20] It is thus not surprising that no significant difference in GSH levels was observed in the current study between patients and control subjects under 'resting' conditions. Furthermore, the absence of prefrontal GSH level difference may reflect a recruitment bias related to the presently studied small sample. Indeed, an independent study showed that the 'GAG high-risk' genotype of the *GCLC* gene predicted lower prefrontal GSH levels.[67] In the genetic association study,[20] larger cohorts were investigated and the 'GAG high-risk' genotypes constituted 39% of the patients, while it is only 20% in the present study, owing to a recruitment bias of a very demanding study. Summing up, both the 'resting' conditions of MRI and the low proportion of 'GAG high-risk' patients in the population investigated explain the absence of GSH difference between patients and controls.

Finally, our study reveals that a GSH deficit causes an impairment of Fyn pathway. A GSH deficit results in decreased

Figure 3. Glutathione (GSH) deficit induced by short hairpin RNA (shRNA) against the catalytic subunit (GCLC) of the glutamate-cysteine ligase reduces proliferation, increases early differentiation but decreases later maturation stage of oligodendrocyte progenitor cells (OPCs). (**a**) Oligodendrocyte cell culture immunostained for NG2 (green) and cell nuclei counterstained with 4′-6-diamidino-2-phenylindole (DAPI) (blue). Scale bar: 50 μm. (**b**) Quantification by western blot of GCLC protein levels in oligodendrocyte cultures treated with either scrambled or GCLC shRNA. GCLC protein levels were normalized to α-tubulin and expressed as the percentage of their respective scrambled shRNA. Bar graphs represent mean ± s.e.m. ($n = 6$). $^{**}P < 0.01$. Student's paired *t*-test. (**c**) GSH levels measured after different infection times: 5, 7 or 10 days (n = 6–7). Values are expressed as the percentage of their respective scrambled shRNA. Bar graphs represent mean ± s.e.m. $^{*}P < 0.05$ and $^{**}P < 0.01$. Student's paired *t*-test. (**d**) Proliferation of OPCs assessed by bromodeoxyuridine (BrdU) incorporation (green) and costained with NG2 (red) and cell nuclei (DAPI: blue). Scale bar: 50 μm. (**e**) Effect of *N*-acetylcysteine (NAC) treatment (24 h) on the number of BrdU-positive among NG2-positive cells. Data are expressed as the percentage of their respective scrambled shRNA ($n = 10$, mean ± s.e.m.). $^{**}P < 0.01$ and $^{***}P < 0.001$, analyzed by Wilcoxon's test for control condition and linear mixed-effect model for multiple comparisons (control vs NAC). (**f** and **g**) Quantification of O4- and CNP-positive cells over total cell nuclei (DAPI) at 7 (**f**) and 10 days (**g**) after infection. Values were expressed as the percentage of their respective control condition. Bar graphs represent mean ± s.e.m. ($n = 6$–7). $^{*}P < 0.05$ and $^{**}P < 0.01$, analyzed by Student's paired *t*-test. (**h**) Quantification of CNP protein levels in cells treated with either scrambled or GCLC shRNA in either proliferating medium (platelet-derived growth factor-AA (PDGF-AA), basic fibroblast growth factor (bFGF)) or differentiating medium (T3). CNP protein levels were normalized to α-tubulin and expressed as the percentage of their respective control condition (PDGF-AA, bFGF). Bar graphs represent mean ± s.e.m. ($n = 5$). $^{**}P < 0.01$, analyzed by Student's paired *t*-test. (**i**) Representative image of MBP labeling (red) and cell nuclei (DAPI: blue) in oligodendrocytes expressing scrambled (top panel) or GCLC shRNA (bottom panel) following T3 incubation. Scale bar: 50 μm. (**j**) Quantification of MBP-positive cells over total cell nuclei after T3 treatment. Values were expressed as the percentage of their respective scrambled shRNA. Bar graphs represent mean ± s.e.m. ($n = 6$). $^{*}P < 0.05$, analyzed by Student's paired *t*-test.

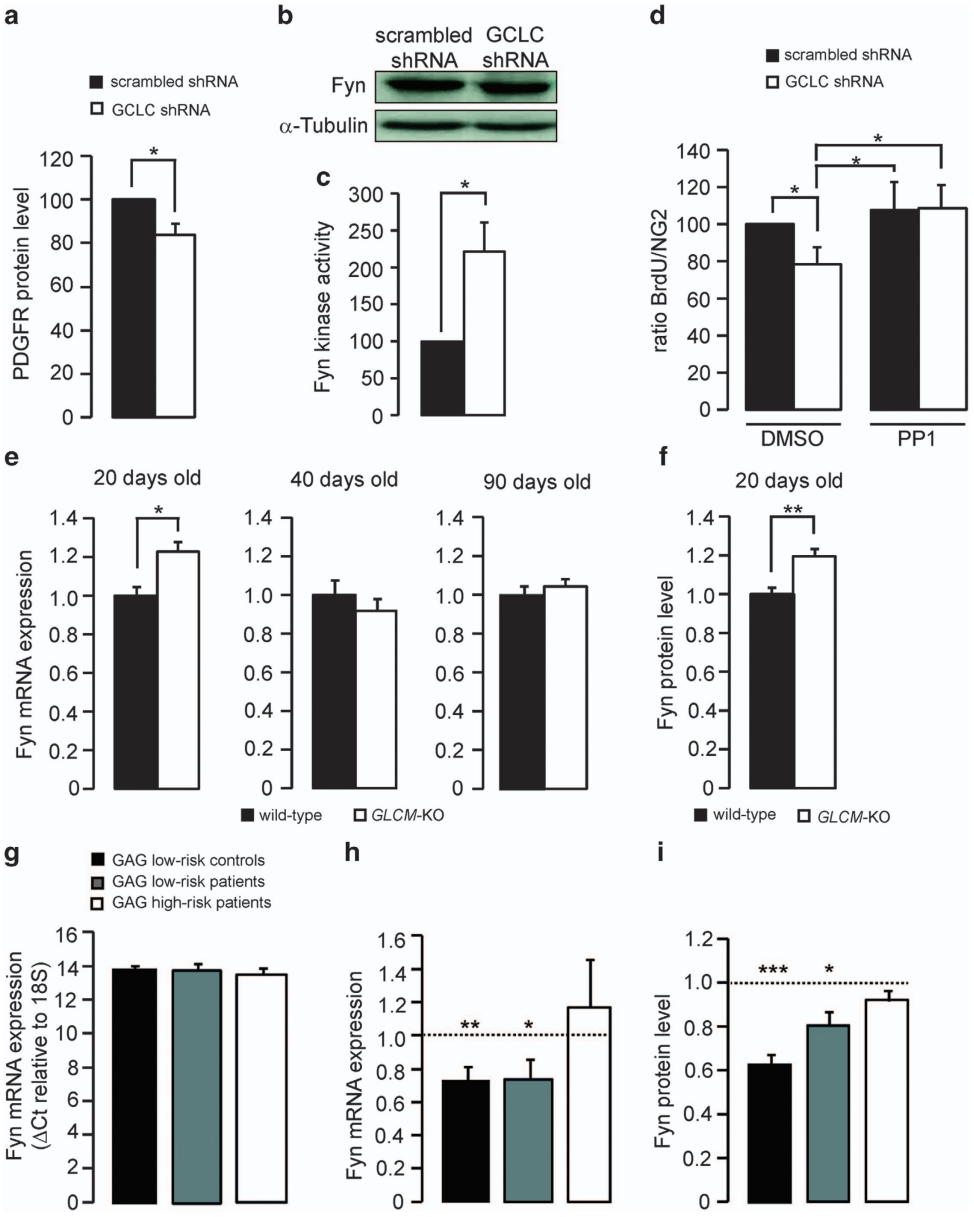

Figure 4. Glutathione (GSH) deficit affects Fyn kinase in rodents and patients. (**a**) Platelet-derived growth factor receptor (PDGFR) protein expression was evaluated by western blot at 7 days after infection ($n = 7$). Protein levels of PDGFR were normalized to α-tubulin and expressed as the percentage of their respective scrambled short hairpin RNA (shRNA) (black bar). Bar graphs represent means of seven different experiments ± s.e.m. $^*P < 0.05$, Student's paired *t*-test. (**b**) Representative western blot of Fyn protein expression at 7 days after infection. (**c**) Analysis of Fyn kinase activity. Bar graphs represent Fyn-dependent ATP consumption, expressed as the percentage of the scrambled condition. Bar graphs represent mean ± s.e.m. ($n = 5$). $^*P < 0.05$, Student's paired *t*-test. (**d**) Effect of Fyn inhibitor (4-amino-5-(methylphenyl)-7-(t-butyl)pyrazolo-(3,4-d)pyrimidine (PP1)) on proliferation assessed by bromodeoxyuridine (BrdU) incorporation. BrdU-positive over NG2-positive cells were quantified after 24-h treatment with PP1 at day 7. Data are expressed as the percentage of their respective scrambled shRNA treated with vehicle (dimethyl sulfoxide (DMSO)) (mean ± s.e.m., $n = 9$). $^*P < 0.05$, linear mixed-effect model. (**e**) Fyn mRNA expression in the anterior cingulate cortex of wild-type and *GCLM*-KO mice, at 20, 40 and 90 days old. Data were expressed as mean ± s.e.m., relative to wild-type mice ($n = 6$–9). $^*P < 0.05$, Wilcoxon's test. (**f**) Quantification by western blot of Fyn protein levels in the anterior cingulate cortex of wild-type and *GCLM*-KO mice, at 20 days old. Fyn protein levels were normalized to β-actin. Data were expressed as mean ± s.e.m., relative to wild-type mice ($n = 6$–8). $^{**}P < 0.01$, Student's *t*-test. (**g**) Fyn mRNA expression assessed by quantitative PCR in vehicle condition (DMSO) in fibroblasts from 'GAG high-risk' patients, 'GAG low-risk' patients or control individuals. Mean ΔCt value is shown in bar graphs (± s.e.m.). (**h**) Fold change in Fyn mRNA expression in fibroblasts following *tert*-butylhydroquinone (tBHQ) treatment. Mean values of fold change relative to DMSO treatment (± s.e.m.). $^*P < 0.05$ and $^{**}P < 0.01$, Student's paired *t*-test or Wilcoxon's test. (**i**) Fibroblast Fyn protein expression was analyzed by western blot following tBHQ treatment. Fyn protein expression was normalized by β-actin. Data were expressed as mean ± s.e.m. ($n = 10$–12), relative to vehicle condition (DMSO). $^*P < 0.05$ and $^{***}P < 0.001$, Student's paired *t*-test or Wilcoxon's test.

proliferation in OPC culture via the upregulation of Fyn kinase activity. Likewise, young *GCLM*-KO mice have an increase in Fyn mRNA and protein expressions in the developing anterior cingulate cortex. The upregulation of Fyn in our *in vitro* and *in vivo* models of GSH deficit is also in line with redox regulation of Fyn activity described in various cell types, including lymphocytes, endothelial cells and fibroblasts.[68,69] It has been proposed that, through redox-sensitive sites, oxidative state conditions inactivate

protein tyrosine phosphatase leading to the upregulation of the activity of Src family including Fyn.[70] Alternatively, upregulation of Fyn mRNA expression may be induced by the activation of redox-sensitive transcription factor Erg1.[71] Interestingly, fibroblasts from early psychosis patients with 'GAG high-risk' genotypes, associated with a vulnerability to redox dysregulation, have impaired regulation of Fyn mRNA and protein expressions during an oxidative challenge (tBHQ). Noteworthy, an increase in Fyn mRNA and protein levels has been also reported in the *post-mortem* prefrontal cortex of schizophrenia patients.[72] Furthermore, the Stanley Neuropathology Consortium Integrative Database (a web-based tool that integrates results of various microarray studies carried out with the Stanley brain array collection: https://www.stanleygenomics.org/) reveals a significant upregulation of Fyn mRNA expression in schizophrenia patients (35 cases *vs* 35 controls). To summarize, the increase of Fyn in a patients' subgroup may result from an impairment in redox regulation, and cause impaired Fyn-mediated signaling pathways that could contribute to developmental abnormalities including oligodendrocyte maturation.

Taken all together, these data suggest the presence of a critical developmental period during which a proper redox regulation and GSH levels are required for myelination processes. Adverse events during early life are risk factors for the psychopathology and myelin development.[73,74] This also suggests that there are several critical periods during which environmental risk factors could impact the normal development of myelin. Indeed, transient changes in GSH levels induced by environmental insults during pre-, peri- and postnatal periods may have an impact on oligodendrocyte maturation, consequently affecting later structural connectivity. In addition to schizophrenia, these findings may be relevant to other GSH-deficit-related psychiatric disorders, including bipolar disorder or major depressive disorder, which are both associated with white matter abnormalities.[18,65]

A better understanding of molecular mechanisms underlying redox control of myelination at various developmental vulnerability periods will pave the way toward new drug targets and strategies for the treatment and prevention of schizophrenia.

CONFLICT OF INTEREST

The authors declare no conflict of interest.

ACKNOWLEDGMENTS

This work was supported by the Swiss National Science Foundation (Grant Nos. 310030_135736/1 to KQD and PS, 320030_122419 to PC and KQD and 130090 to PH) and the National Center of Competence in Research (NCCR) 'SYNAPSY—The Synaptic Bases of Mental Diseases' (Grant No. 51AU40_125759). We thank the Brazilian Swiss Joint Research Program (BSJRP), the 'Loterie Romande', Damm-Etienne Foundation, Avina Foundation and Alamaya Foundation. PH was financially supported by Leenaards Foundation. We are grateful for technical assistance to Hélène Moser and Adeline Cottier. We also thank Dr Mehdi Gholam for advices on statistics, Dr Portia Vliet for the GCLC antibody and Dr Ibro Ambeskovic for advices on OPC culture and *in vitro* experiments. We extend thanks to Ying Chen for providing us with the *GCLM*-KO breeders. Most of all, we express our gratitude to all patients and healthy volunteers for their enduring participation.

AUTHOR CONTRIBUTIONS

AM wrote the manuscript, designed and carried out the rodent experiments and performed human fibroblast culture. PSB wrote the manuscript and performed the patient recruitment and skin biopsy and analyzed DSI. AG performed DSI/fMRI acquisition and analyzed the data. LX and RM performed MRS acquisition and analyzed the data. MF wrote the manuscript, designed and performed human fibroblast culture and evaluated data from Stanley database. CB designed and prepared shRNA. MK established OPC culture. J-HC contributed to morphology analysis of *GCLM*-KO mice and editing the manuscript. PS designed and contributed to experiments in rodents and to the manuscript writing. CF recruited control subjects and early psychosis patients and performed psychiatric evaluations. MC contributed to the overall study concept and to the manuscript writing. RG supervised MRS study. J-PT supervised DSI/fMRI analysis. PH designed, analyzed and supervised DSI/fMRI study. PC contributed to the overall concept, and planned and coordinated the recruitment in human study. KQD conceived and directed the whole study, and contributed to the writing. All authors reviewed and edited the manuscript.

REFERENCES

1 Davis KL, Stewart DG, Friedman JI, Buchsbaum M, Harvey PD, Hof PR, *et al.* White matter changes in schizophrenia: evidence for myelin-related dysfunction. *Arch Gen Psychiatry* 2003; **60**: 443–456.
2 Hakak Y, Walker JR, Li C, Wong WH, Davis KL, Buxbaum JD, *et al.* Genome-wide expression analysis reveals dysregulation of myelination-related genes in chronic schizophrenia. *Proc Natl Acad Sci USA* 2001; **98**: 4746–4751.
3 Katsel P, Davis KL, Haroutunian V. Variations in myelin and oligodendrocyte-related gene expression across multiple brain regions in schizophrenia: a gene ontology study. *Schizophr Res* 2005; **79**: 157–173.
4 Hof PR, Haroutunian V, Copland C, Davis KL, Buxbaum JD. Molecular and cellular evidence for an oligodendrocyte abnormality in schizophrenia. *Neurochem Res* 2002; **27**: 1193–1200.
5 Stark AK, Uylings HB, Sanz-Arigita E, Pakkenberg B. Glial cell loss in the anterior cingulate cortex, a subregion of the prefrontal cortex, in subjects with schizophrenia. *Am J Psychiatry* 2004; **161**: 882–888.
6 Uranova NA, Vostrikov VM, Vikhreva OV, Zimina IS, Kolomeets NS, Orlovskaya DD. The role of oligodendrocyte pathology in schizophrenia. *Int J Neuropsychopharmacol* 2007; **10**: 537–545.
7 Du F, Cooper A, Cohen BM, Renshaw PF, Ongur D. Water and metabolite transverse T2 relaxation time abnormalities in the white matter in schizophrenia. *Schizophr Res* 2012; **137**: 241–245.
8 Kubicki M, Westin CF, McCarley RW, Shenton ME. The application of DTI to investigate white matter abnormalities in schizophrenia. *Ann NY Acad Sci* 2005; **1064**: 134–148.
9 Kyriakopoulos M, Bargiotas T, Barker GJ, Frangou S. Diffusion tensor imaging in schizophrenia. *Eur Psychiatry* 2008; **23**: 255–273.
10 Jones DP. Radical-free biology of oxidative stress. *Am J Physiol Cell Physiol* 2008; **295**: C849–C868.
11 Bitanihirwe BK, Woo TU. Oxidative stress in schizophrenia: an integrated approach. *Neurosci Biobehav Rev* 2011; **35**: 878–893.
12 Do KQ, Cabungcal JH, Frank A, Steullet P, Cuenod M. Redox dysregulation, neurodevelopment, and schizophrenia. *Curr Opin Neurobiol* 2009; **19**: 220–230.
13 Reddy R, Keshavan M, Yao JK. Reduced plasma antioxidants in first-episode patients with schizophrenia. *Schizophr Res* 2003; **62**: 205–212.
14 Yao JK, Keshavan MS. Antioxidants, redox signaling, and pathophysiology in schizophrenia: an integrative view. *Antioxidants Redox Signal* 2011; **15**: 2011–2035.
15 Meister A, Anderson ME. Glutathione. *Annu Rev Biochem* 1983; **52**: 711–760.
16 Do KQ, Trabesinger AH, Kirsten-Kruger M, Lauer CJ, Dydak U, Hell D, *et al.* Schizophrenia: glutathione deficit in cerebrospinal fluid and prefrontal cortex *in vivo*. *Eur J Neurosci* 2000; **12**: 3721–3728.
17 Matsuzawa D, Hashimoto K. Magnetic resonance spectroscopy study of the antioxidant defense system in schizophrenia. *Antioxidants Redox Signal* 2011; **15**: 2057–2065.
18 Gawryluk JW, Wang JF, Andreazza AC, Shao L, Young LT. Decreased levels of glutathione, the major brain antioxidant, in post-mortem prefrontal cortex from patients with psychiatric disorders. *Int J Neuropsychopharmacol* 2011; **14**: 123–130.
19 Gravina P, Spoletini I, Masini S, Valentini A, Vanni D, Paladini E, *et al.* Genetic polymorphisms of glutathione *S*-transferases GSTM1, GSTT1, GSTP1 and GSTA1 as risk factors for schizophrenia. *Psychiatry Res* 2011; **187**: 454–456.
20 Gysin R, Kraftsik R, Sandell J, Bovet P, Chappuis C, Conus P, *et al.* Impaired glutathione synthesis in schizophrenia: convergent genetic and functional evidence. *Proc Natl Acad Sci USA* 2007; **104**: 16621–16626.
21 Rodriguez-Santiago B, Brunet A, Sobrino B, Serra-Juhe C, Flores R, Armengol L, *et al.* Association of common copy number variants at the glutathione S-transferase genes and rare novel genomic changes with schizophrenia. *Mol Psychiatry* 2010; **15**: 1023–1033.
22 Tosic M, Ott J, Barral S, Bovet P, Deppen P, Gheorghita F *et al.* Schizophrenia and oxidative stress: glutamate cysteine ligase modifier as a susceptibility gene. *American journal of human genetics* 2006; **79**: 586–592.
23 Gokhale A, Larimore J, Werner E, So L, Moreno-De-Luca A, Lese-Martin C, *et al.* Quantitative proteomic and genetic analyses of the schizophrenia susceptibility

factor dysbindin identify novel roles of the biogenesis of lysosome-related organelles complex 1. *J Neurosci* 2012; **32**: 3697–3711.
24 Goldshmit Y, Erlich S, Pinkas-Kramarski R. Neuregulin rescues PC12-ErbB4 cells from cell death induced by H(2)O(2). Regulation of reactive oxygen species levels by phosphatidylinositol 3-kinase. *J Biol Chem* 2001; **276**: 46379–46385.
25 Johnson AW, Jaaro-Peled H, Shahani N, Sedlak TW, Zoubovsky S, Burruss D, *et al.* Cognitive and motivational deficits together with prefrontal oxidative stress in a mouse model for neuropsychiatric illness. *Proc Natl Acad Sci USA* 2013; **110**: 12462–12467.
26 Krishnan N, Dickman MB, Becker DF. Proline modulates the intracellular redox environment and protects mammalian cells against oxidative stress. *Free Radic Biol Med* 2008; **44**: 671–681.
27 Otte DM, Sommersberg B, Kudin A, Guerrero C, Albayram O, Filiou MD, *et al. N*-acetyl cysteine treatment rescues cognitive deficits induced by mitochondrial dysfunction in G72/G30 transgenic mice. *Neuropsychopharmacology* 2011; **36**: 2233–2243.
28 Gysin R, Kraftsik R, Boulat O, Bovet P, Conus P, Comte-Krieger E, *et al.* Genetic dysregulation of glutathione synthesis predicts alteration of plasma thiol redox status in schizophrenia. *Antioxidants Redox Signal* 2011; **15**: 2003–2010.
29 Steullet P, Cabungcal JH, Kulak A, Kraftsik R, Chen Y, Dalton TP, *et al.* Redox dysregulation affects the ventral but not dorsal hippocampus: impairment of parvalbumin neurons, gamma oscillations, and related behaviors. *J Neurosci* 2010; **30**: 2547–2558.
30 Cabungcal JH, Steullet P, Kraftsik R, Cuenod M, Do KQ. Early-life insults impair parvalbumin interneurons via oxidative stress: reversal by *N*-acetylcysteine. *Biol Psychiatry* 2012; **73**: 574–582.
31 Kulak A, Cuenod M, Do KQ. Behavioral phenotyping of glutathione-deficient mice: relevance to schizophrenia and bipolar disorder. *Behav Brain Res* 2012; **226**: 563–570.
32 Thorburne SK, Juurlink BH. Low glutathione and high iron govern the susceptibility of oligodendroglial precursors to oxidative stress. *J Neurochem* 1996; **67**: 1014–1022.
33 Jana M, Pahan K. Down-regulation of myelin gene expression in human oligodendrocytes by nitric oxide: implications for demyelination in multiple sclerosis. *J Clin Cell Immunol* 2013; **4**.
34 Back SA, Gan X, Li Y, Rosenberg PA, Volpe JJ. Maturation-dependent vulnerability of oligodendrocytes to oxidative stress-induced death caused by glutathione depletion. *J Neurosci* 1998; **18**: 6241–6253.
35 Cavaliere F, Urra O, Alberdi E, Matute C. Oligodendrocyte differentiation from adult multipotent stem cells is modulated by glutamate. *Cell Death Dis* 2012; **3**: e268.
36 Smith J, Ladi E, Mayer-Proschel M, Noble M. Redox state is a central modulator of the balance between self-renewal and differentiation in a dividing glial precursor cell. *Proc Natl Acad Sci USA* 2000; **97**: 10032–10037.
37 Yung AR, Yuen HP, McGorry PD, Phillips LJ, Kelly D, Dell'Olio M, *et al.* Mapping the onset of psychosis: the comprehensive assessment of at-risk mental states. *Aust NZ J Psychiatry* 2005; **39**: 964–971.
38 Baumann PS, Crespi S, Marion-Veyron R, Solida A, Thonney J, Favrod J, *et al.* Treatment and early intervention in psychosis program (TIPP-Lausanne): implementation of an early intervention programme for psychosis in Switzerland. *Early Interv Psychiatry* 2013; **7**: 322–328.
39 Nurnberger JI Jr, Blehar MC, Kaufmann CA, York-Cooler C, Simpson SG, Harkavy-Friedman J, *et al.* Diagnostic interview for genetic studies. Rationale, unique features, and training. NIMH Genetics Initiative. Archives of general psychiatry. 1994; **51**: 849–859; discussion 63-4.
40 Wedeen VJ, Hagmann P, Tseng WY, Reese TG, Weisskoff RM. Mapping complex tissue architecture with diffusion spectrum magnetic resonance imaging. *Magn Reson Med* 2005; **54**: 1377–1386.
41 Daducci A, Gerhard S, Griffa A, Lemkaddem A, Cammoun L, Gigandet X, *et al.* The connectome mapper: an open-source processing pipeline to map connectomes with MRI. *PLoS One* 2012; **7**: e48121.
42 Richiardi J, Eryilmaz H, Schwartz S, Vuilleumier P, Van De Ville D. Decoding brain states from fMRI connectivity graphs. *NeuroImage* 2011; **56**: 616–626.
43 Desikan RS, Segonne F, Fischl B, Quinn BT, Dickerson BC, Blacker D, *et al.* An automated labeling system for subdividing the human cerebral cortex on MRI scans into gyral based regions of interest. *NeuroImage* 2006; **31**: 968–980.
44 Greicius MD, Supekar K, Menon V, Dougherty RF. Resting-state functional connectivity reflects structural connectivity in the default mode network. *Cereb Cortex* 2009; **19**: 72–78.
45 Gruetter R. Automatic, localized *in vivo* adjustment of all first- and second-order shim coils. *Magn Reson Med* 1993; **29**: 804–811.
46 Mekle R, Mlynarik V, Gambarota G, Hergt M, Krueger G, Gruetter R. MR spectroscopy of the human brain with enhanced signal intensity at ultrashort echo times on a clinical platform at 3T and 7T. *Magn Reson Med* 2009; **61**: 1279–1285.
47 Mlynarik V, Gambarota G, Frenkel H, Gruetter R. Localized short-echo-time proton MR spectroscopy with full signal-intensity acquisition. *Magn Reson Med* 2006; **56**: 965–970.
48 Provencher SW. Estimation of metabolite concentrations from localized *in vivo* proton NMR spectra. *Magn Reson Med* 1993; **30**: 672–679.
49 Xin L, Gambarota G, Mlynarik V, Gruetter R. Proton T2 relaxation time of J-coupled cerebral metabolites in rat brain at 9.4T. *NMR Biomed* 2008; **21**: 396–401.
50 Yang Y, Dieter MZ, Chen Y, Shertzer HG, Nebert DW, Dalton TP. Initial characterization of the glutamate-cysteine ligase modifier subunit Gclm(−/−) knockout mouse. Novel model system for a severely compromised oxidative stress response. *J Biol Chem* 2002; **277**: 49446–49452.
51 McCarthy KD, de Vellis J. Preparation of separate astroglial and oligodendroglial cell cultures from rat cerebral tissue. *J Cell Biol* 1980; **85**: 890–902.
52 Cabungcal JH, Nicolas D, Kraftsik R, Cuenod M, Do KQ, Hornung JP. Glutathione deficit during development induces anomalies in the rat anterior cingulate GABAergic neurons: relevance to schizophrenia. *Neurobiol Dis* 2006; **22**: 624–637.
53 Franklin BJ, Paxinos G. *The Mouse Brain in Stereotaxic Coordinates*. 3rd edn. New York, NY, USA: Academic Press, 2008.
54 Livak KJ, Schmittgen TD. Analysis of relative gene expression data using real-time quantitative PCR and the 2(−Delta Delta C(T)) Method. *Methods* 2001; **25**: 402–408.
55 Lowe MJ, Mock BJ, Sorenson JA. Functional connectivity in single and multislice echoplanar imaging using resting-state fluctuations. *NeuroImage* 1998; **7**: 119–132.
56 Lebel C, Beaulieu C. Longitudinal development of human brain wiring continues from childhood into adulthood. *J Neurosci* 2011; **31**: 10937–10947.
57 Li Z, Dong T, Proschel C, Noble M. Chemically diverse toxicants converge on Fyn and c-Cbl to disrupt precursor cell function. *PLoS Biol* 2007; **5**: e35.
58 Noble M, Smith J, Power J, Mayer-Proschel M. Redox state as a central modulator of precursor cell function. *Ann NY Acad Sci* 2003; **991**: 251–271.
59 French HM, Reid M, Mamontov P, Simmons RA, Grinspan JB. Oxidative stress disrupts oligodendrocyte maturation. *J Neurosci Res* 2009; **87**: 3076–3087.
60 Beaulieu C. The basis of anisotropic water diffusion in the nervous system—a technical review. *NMR Biomed* 2002; **15**: 435–455.
61 Bartzokis G. Schizophrenia: breakdown in the well-regulated lifelong process of brain development and maturation. *Neuropsychopharmacology* 2002; **27**: 672–683.
62 Harris LW, Lockstone HE, Khaitovich P, Weickert CS, Webster MJ, Bahn S. Gene expression in the prefrontal cortex during adolescence: implications for the onset of schizophrenia. *BMC Med Genom* 2009; **2**: 28.
63 Kolb B, Mychasiuk R, Muhammad A, Li Y, Frost DO, Gibb R. Experience and the developing prefrontal cortex. *Proc Natl Acad Sci USA* 2012; **109**(Suppl 2): 17186–17193.
64 Blakemore SJ, Choudhury S. Development of the adolescent brain: implications for executive function and social cognition. *J Child Psychol Psychiatry Allied Disc* 2006; **47**: 296–312.
65 Fields RD. White matter in learning, cognition and psychiatric disorders. *Trends Neurosci* 2008; **31**: 361–370.
66 Nave KA. Myelination and support of axonal integrity by glia. *Nature* 2010; **468**: 244–252.
67 Xin L, Mekle R, Ferrari C, Baumann PS, Alameda L, Moser H, *et al.* Genetic association with prefrontal glutathione deficit: a preliminary 3T1H MRS Study in Early Psychosis. *Proceedings of the International Society of Magnetic Resonance in Medicine Annual Meeting and Exhibition*, 10–16 May; Milan, Italy, 2014.
68 Abe J, Okuda M, Huang Q, Yoshizumi M, Berk BC. Reactive oxygen species activate p90 ribosomal S6 kinase via Fyn and Ras. *J Biol Chem* 2000; **275**: 1739–1748.
69 Sanguinetti AR, Cao H, Corley Mastick C. Fyn is required for oxidative- and hyperosmotic-stress-induced tyrosine phosphorylation of caveolin-1. *Biochem J* 2003; **376**(Part 1): 159–168.
70 Salmeen A, Barford D. Functions and mechanisms of redox regulation of cysteine-based phosphatases. *Antioxid Redox Signal* 2005; **7**: 560–577.
71 Gao Y, Howard A, Ban K, Chandra J. Oxidative stress promotes transcriptional up-regulation of Fyn in BCR-ABL1-expressing cells. *J Biol Chem* 2009; **284**: 7114–7125.
72 Ohnuma T, Kato H, Arai H, McKenna PJ, Emson PC. Expression of Fyn, a non-receptor tyrosine kinase in prefrontal cortex from patients with schizophrenia and its correlation with clinical onset. *Brain Res Mol Brain Res* 2003; **112**: 90–94.
73 Eluvathingal TJ, Chugani HT, Behen ME, Juhasz C, Muzik O, Maqbool M, *et al.* Abnormal brain connectivity in children after early severe socioemotional deprivation: a diffusion tensor imaging study. *Pediatrics* 2006; **117**: 2093–2100.
74 Huang H, Gundapuneedi T, Rao U. White matter disruptions in adolescents exposed to childhood maltreatment and vulnerability to psychopathology. *Neuropsychopharmacology* 2012; **37**: 2693–2701.

Supplementary Information accompanies the paper on the Molecular Psychiatry website (http://www.nature.com/mp)